Reduced Dark Current With a Specific Detectivity Advantage in Extended Threshold Wavelength Infrared Detector

Article · May 2019

DOI: 10.1109/LSENS.2019.2915016

Divya Somvanshi
Technion - Israel Institute of Technology

Dilip Chauhan
Georgia State University

A. G. U. Perera
Georgia State University

L. H. Li
University of Leeds

IEEE Sensors Letters VOL. 3, NO. 5, MAY 2019 3501004

Electromagnetic wave sensors

Reduced Dark Current With a Specific Detectivity Advantage in Extended Threshold Wavelength Infrared Detector

Divya Somvanshi[1,2,*], Dilip Chauhan[1], A. G. Unil Perera[1,**], Lianhe Li[3], Li Chen[3], and Edmund H. Linfield[3]

[1]Center for Nano-Optics, Department of Physics and Astronomy, Georgia State University, Atlanta, GA 30303 USA
[2]The Department of Electronics and Tele-Communication Engineering, Jadavpur University, Kolkata 700032, India
[3]School of Electronic and Electrical Engineering, University of Leeds, Leeds LS2 9JT, U.K.
[*]Member, IEEE
[**]Fellow, IEEE

Manuscript received April 12, 2019; accepted April 30, 2019. Date of publication May 6, 2019; date of current version May 22, 2019.

Abstract—Reduced dark current leading to a specific detectivity (D*) advantage over conventional detectors for extended threshold wavelength (ET) detectors are reported in this article. For an infrared (IR) detector with a graded injector barrier and barrier energy offset, the measured dark current was found to agree well with theoretical fits obtained from a 3-D carrier drift model using the designed value of $\Delta = 0.40$ eV ($\lambda_t = 3.1$ μm) (where $\Delta = 1.24/\lambda_t$, Δ is the internal work function and λ_t is the corresponding threshold wavelength), whereas the effective photoresponse threshold wavelength determined from the spectral response measurements corresponds to 13.7 μm at 50 K. However, for the conventional detectors, both the dark current and photoresponse threshold agree very well with the designed value of Δ. Comparing threshold wavelengths of an ET detector and a conventional detector, an advantage in D* is observed for ET detectors due to the strong reduction in dark current. Using this idea, standard threshold semiconductor detectors could be designed to operate as long wavelength detectors with a higher value of detectivity and dark current (corresponding to the original short-wavelength threshold).

Index Terms—Electromagnetic wave sensors, dark current, detectivity, GaAs/AlGaAs heterostructures, infrared (IR) photodetectors, optoelectronic sensors.

I. INTRODUCTION

Dark current is an unavoidable fact in any photoconductive detector. A common technique to reduce the dark current is to lower the operating temperature, making the detector operation costlier and cumbersome. Therefore, reducing the dark current without cooling will be an advantage, especially for longer wavelength detectors for next-generation optoelectronic devices.

In general, the threshold wavelength (λ_t) of a conventional detector is determined by the relation [1]–[3] $\lambda_t = 1.24/\Delta$, where Δ is the internal work function associated with growth, design, and also with the dark current [5]. The internal work function is defined as the energy difference between the valence band edge of the barrier bottom and the Fermi level of emitter [3]. However, in an IR detector with graded barrier and a barrier energy offset (δE_v) [3], [6], i.e., extended threshold wavelength (ET) detector, the dark current depends upon Δ, while photoresponse threshold wavelength from the spectral response (λ_{eff}) is governed by an effective work function, i.e., $\Delta' = 1.24/\lambda_{\text{eff}}$ ($\Delta' << \Delta$), where λ_{eff} is beyond the standard expected limit set by λ_t [3], [7]–[9]. Recently, for an ET detector, the measured dark current was found to agree well with the designed value of $\Delta = 0.40$ eV (3.1 μm), whereas the experimental spectral photoresponse showed [5] extended threshold wavelengths (λ_{eff}) of 68, 45, and 60 μm at positive, zero, and negative voltage biases, respectively, at temperature 5.3 K. An ET detector consists of p-GaAs/$Al_xGa_{1-x}As$ heterostructure with an absorber/emitter (p-type GaAs) sandwiched between high energy undoped $Al_xGa_{1-x}As$ graded barrier and low energy undoped $Al_xGa_{1-x}As$ constant barrier, the energy difference between the barriers is referred to as the barrier energy offset (δE_v). The detection mechanism involves free carrier absorption in the emitter layer, followed by the internal photoemission of photoexcited carriers across the junction and then collection across the barrier. The model used to explain the observation of λ_{eff} in ET detectors is based on the hot carrier effects [10], [11], as reported by Somvanshi *et al*. [12]. The interactions of hot carriers in doped GaAs layers were extensively studied in the past experimentally, as well as theoretically [13], [14].

Nowadays, there has been an increased interest in using hot-carrier driven effects for various photodetection and light-harvesting applications [15], [16]. Therefore, the development of ET detectors based on hot-carrier effects, which overcome the restriction imposed on λ_t by Δ is of vital importance. However, for practical applications, to provide an advantage over the conventional detector, an ET detector should have a reduced dark current and also specific detectivity (D*) that is comparable or better than the conventional detector. This article demonstrates that the ET detector with reduced dark current, giving a D* advantage over the conventional detector provides a foundation for the future IR detector applications.

Corresponding authors: Divya Somvanshi and A. G. Unil Perera (email: divya.somvanshi@jadavpuruniversity.in; uperera@gsu.edu).
Associate Editor: M. Kraft.
Digital Object Identifier 10.1109/LSENS.2019.2915016

II. EXPERIMENTAL DETAILS

A set of samples consisting of conventional detectors named SP1, SP2, HE0204 and an ET detector, i.e., 15SP3 were studied. The fabrication and structural details of conventional detectors are shown in Fig. 1(a) and reported in the literature in detail [4], [7], [17]. The ET

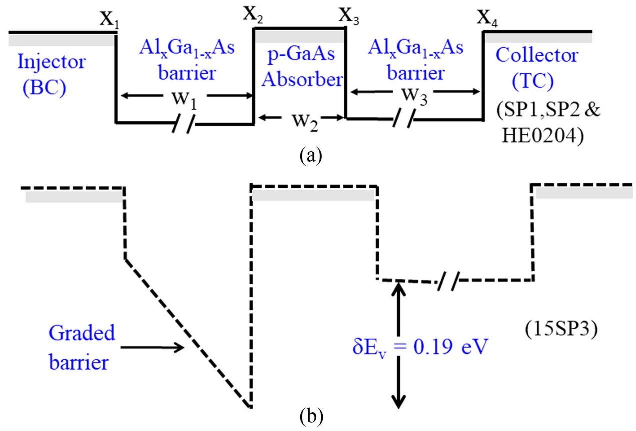

Fig. 1. (a) Unbiased valance band (VB) diagram of conventional detector (denoted by solid lines), where X_1, X_2, X_3, and X_4 are the mole fraction of Al in the $Al_xGa_{1-x}As$ barrier, w_1, w_2, and w_3 are the thicknesses of injector, absorber, and collector, for conventional detectors, value of $X_1 = X_2 = X_3 = X_4$ and are listed in Table I. (b) VB diagram of ET detector, i.e., 15SP3 (denoted by dashed lines), δE_v is the barrier energy offset. In ET detector 15SP3, bottom contact (BC) graded by tuning the Al mole fraction from $X_1 = 0.45$ to $X_2 = 0.75$, and an $Al_{0.39}Ga_{0.61}$ collector barrier is top contact, with $X_3 = X_4 = 0.39$, $w_1 = w_2 = 80$ nm, $w_3 = 400$ nm, N = 1, and $\delta E_v = 0.19$ eV.

Table 1. Structural Details for Listed IR Detectors: Aluminum Mole Fractions (X_1, X_2, X_3, X_4), Barrier Energy Offset (δE_v), Activation Energy from the Dark Current Fitting (Δ), Activation Energy from Experimental Photoresponse (Δ'), and References From Where Data Have Been Taken.

Sample	Al mole fraction				δE_v	Δ	Δ'	Ref
	X_1	X_2	X_3	X_4	(eV)	(eV)	(eV)	
SP1	0.28	0.28	0.28	0.28	0	0.154	0.144	[1]
SP2	0.37	0.37	0.37	0.37	0	0.211	0.190	[1]
HE0204	0.12	0.12	0.12	0.12	0	0.077	0.077	[4]
15SP3	0.45	0.75	0.39	0.39	0.19	0.40	0.091	[5]
M	0.22	0.22	0.22	0.22	0	0.091	0.091	

detector, i.e., 15SP3 were grown by Molecular Beam Epitaxy on semi-insulating GaAs substrates, have three p-type GaAs regions, i.e., bottom contact (BC), absorber (emitter), and top contact (TC), as shown in Fig. 1(b). The 15SP3 consists of the p-GaAs absorber of 80 nm with the bottom and top contacts having thicknesses of 80 and 400 nm, respectively. Detector 15SP3 have a high energy graded barrier and constant low-energy barrier with $\delta E_v = 0.19$ eV. By varying the Al fractions from 0.45 to 0.75, the detector 15SP3 has a graded barrier profile with an energy offset between the barriers below and above the absorber. The valence band (VB) diagram of conventional detectors, i.e., SP1, SP2, and HE0204 (by solid lines) and 15SP3 (dash lines), are shown in Fig. 1(a) and (b). The other details about both the structures are listed in Table I. In addition, device parameters and photoresponse details of a conventional hypothetical detector (M) (which is designed to have a λ_t close to that of 15SP3) are also given in Table I. By partially etching the top contact layer (p-GaAs), an optical window was opened for normal incidence optical illumination of the detectors. The detectors were mounted on the cold head of the liquid nitrogen-cooled Dewar and liquid helium-cooled cryostat to allow measurements of spectral response and dark current. The current–voltage (I-V) characteristics of the photodetectors were measured using a Keithley 2400 source meter; a positive voltage connected to the TC with the BC grounded is referred to as a positive bias. Similarly, a positive voltage connected to the BC with the TC grounded is referred to as a negative bias. A Fourier transform infrared (IR) (Perkin Elmer System 2000 FTIR) spectrometer was used to measure the spectral photoresponse, and a commercial Si composite bolometer (from IR Laboratories, http://www.infraredlaboratories.com/Bolometers.html) with known sensitivity was used to calibrate the photoresponse. More details about both detectors can be found in [4] and [7].

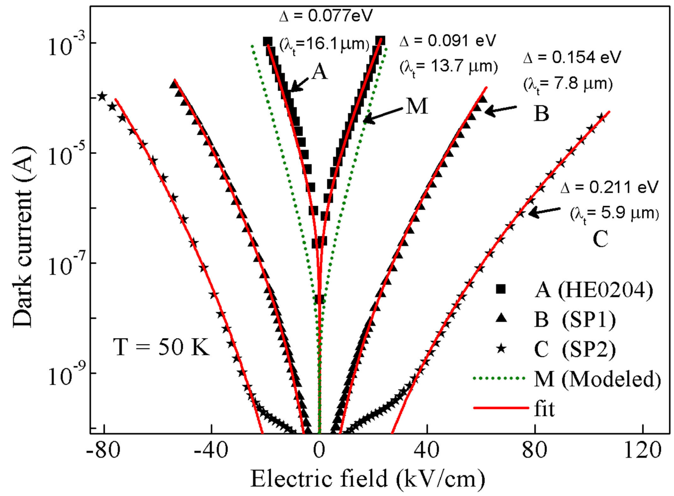

Fig. 2. Experimental (symbol) and dark current curves fitted (red solid line) for the detectors HE0204, SP1, and SP2. In addition, simulated dark current curve for a modeled hypothetical detector (••• M) of 13.7 μm threshold using 3-D drift model.

III. RESULTS AND DISCUSSION

In general, the dark current of the conventional detector is described by a 3-D carrier drift model as [2], [5]

$$I_{dark} = 2Aev(F)\left(\frac{m^* k_B T}{2\pi \hbar^2}\right)^{3/2} \exp\left(-\frac{\Delta - \alpha F}{k_B T}\right) \tag{1}$$

where A is the electrically active area of the detector, e is the electronic charge, Δ is the standard activation energy, $v(F)$ is the carrier drift velocity as a function of electric field, m^* is the effective mass, k_B is Boltzmann's constant, T is temperature, $\hbar$ is the reduced Planck's constant, and α is a fitting parameter that determines effective barrier lowering [2] due to the applied electric field. From (1), it is clear that for a given value of the electric field, $I_{\text{dark}} \propto T^{3/2}\exp(-\Delta/kT)$. Recently, a theoretical model for dark current fitting was reported [5], where dark current is fitted by Δ using 3-D carrier drift model. On the basis of that theoretical model [5], the experimental dark current of detectors SP1, SP2, and HE0204 were fitted using (1), as shown in Fig. 2. The fitted dark current (solid red lines) and the experimentally measured dark current (symbols) are showing excellent agreement. The photoresponse spectra for listed samples were already published previously by our group as reported in [1], [4], [5], and [7], which have λ_t (Δ) of 6.0 μm (0.20 eV) for SP2 [1], 8.2 μm (0.50 eV) for SP1 [1], and 16.1 μm (0.077 eV) for HE0204 [4], respectively, which agree very well with Δ used for dark current model. On the basis of the 3-D dark current model, the dark current of a hypothetical conventional detector (M) for $\Delta = 0.091$ eV is also simulated; the used parameters for simulation are listed in Table I. The simulated dark current for a conventional modeled detector (labeled as M) of $\Delta = 0.091$ eV (13.7 μm) is also shown by the dotted (•••) green line, as shown in Fig. 2. The modeled detector has a reasonable dark current (lower

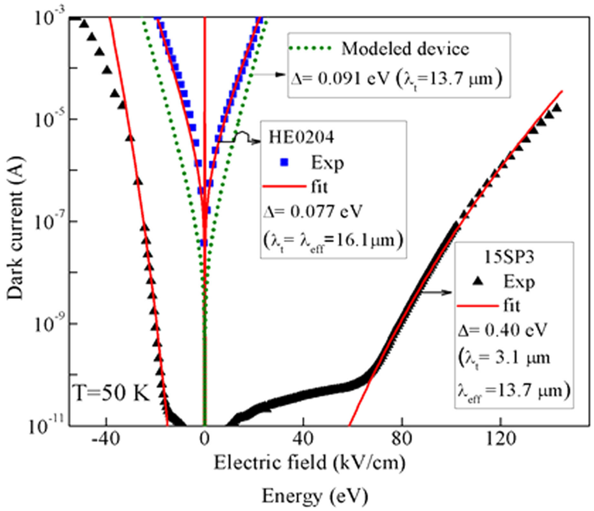

(a)

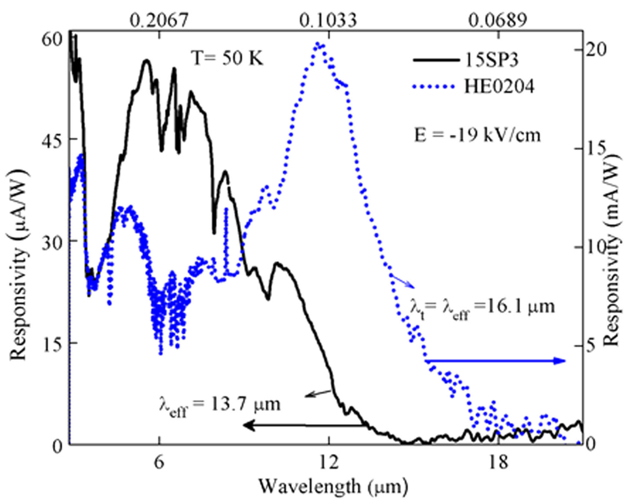

(b)

Fig. 3. (a) Comparison of dark current for detectors HE0204 and 15SP3. A clear difference is seen in dark current for the two detectors for close value of threshold wavelength. A dotted (green) line shows a modeled dark current of a conventional detector with $\Delta = 0.091$ eV ($\lambda_t = 13.7\mu$m). Clearly, the modeled detector has a higher dark current compared to the ET detector with the same value of $\lambda_{\text{eff}} = 13.7\,\mu$m. (b) Photoresponse spectra of HE0204 with $\lambda_t = \lambda_{\text{eff}} = 16.1\ \mu$m ($\Delta' = 0.077$ eV) and dark current also fitted with $\Delta' = 0.077$ eV; however, for 15SP3, $\Delta'(\lambda_{\text{eff}})$ is 0.091 eV (13.7 μm), whereas dark current is fitted with $\Delta = 0.40$ eV corresponding to $\lambda_t = 3.1\ \mu$m

than 16.1 μm and much higher than 7.8 μm detectors) for a 13.7 μm detector. These agreements clearly indicate that the 3-D dark current model is a reasonable model to obtain the dark current of detectors for a given value of Δ.

Now, to demonstrate the dark current advantage in ET detector (15SP3) over the conventional detector, the experimental dark current of 15SP3, HE0204, and modeled (M) detector are compared at 50 K, as shown in Fig. 3(a). The measured dark current of detectors HE0204 and 15SP3 are fitted using (1), as shown in Fig. 3(a), where the solid lines represent the theoretical fits based on the 3-D drift model. The Δ values used for dark current fitting for HE0204 is $\Delta = 0.077$ eV, which corresponds to $\lambda_t = 16.1\ \mu$m and for 15SP3 and $\Delta = 0.40$ eV, which corresponds to $\lambda_t = 3.1\ \mu$m. The experimental photoresponse spectra of both detectors HE0204 and 15SP3 at 50 K are shown in

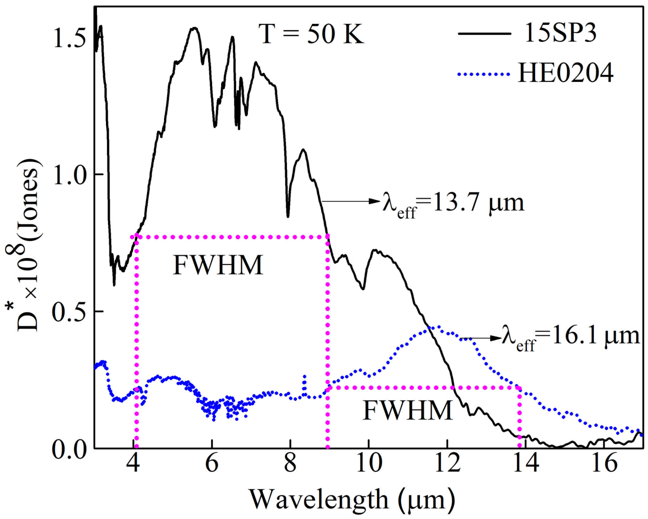

Fig. 4. Comparison of D* for HE0204 and 15SP3 at 50 K; the FWHM value of D* is also included and denoted by dashed lines.

Fig. 3(b) at the electric field (E) $= -19$ kV/cm (since both have different thicknesses and number of periods). The threshold energy of spectral photoresponse is determined by temperature-dependent internal photoemission spectroscopy (TDIPS); the details of the TDIPS principle and the formalism for interpreting yield spectra by a fitting procedure are described in [18]. From Fig. 3(a) and (b), it is observed that Δ value used for dark current fittings for HE0204 is $\Delta = 0.077$ eV corresponds to $\lambda_t = 16.1\ \mu$m, which matches very well with experimental threshold wavelength of HE0204. Although, for 15SP3, the Δ values used for dark current fitting is $\Delta = 0.40$ eV ($\lambda_t = 3.1\ \mu$m); however, 15SP3 shows an experimental photoresponse of $\Delta = 0.091$ eV corresponding to λ_{eff} of 13.7 μm. Clearly, 15SP3 shows a dark current of a 3.1 μm detector, whereas photoresponse corresponds to a 13.7 μm detector, which means 15SP3 have reduced dark current advantage as compared to the conventional detector with the close value of the photoresponse threshold wavelength. Since the existing conventional detector has $\lambda_t = 16.1\ \mu$m (HE0204), a modeled hypothetical detector with a $\lambda_t = 13.7\ \mu$m is used for justifying the dark current advantage. Clearly, the dark current of 15SP3 is also much lower than that of both $\lambda_t = 16.1\ \mu$m threshold detector and the simulated dark current of the modeled device with $\lambda_t = 13.7\ \mu$m. This confirms the dark current advantage in ET detector, i.e., 15SP3 as compared to conventional detector HE0204. From the photoresponse spectra of HE0204 and 15SP3 [see Fig. 3(b)], the value of peak responsivity is calculated. It is observed that peak responsivity (R) of the 15SP3 is equal to 56.6 μA/W at 5.5 μm, which is much lower as compared to the detector HE0204 that has R ~20.3 mA/W at 11.6 μm.

The D* for both detectors, i.e., 15SP3 and HE0204 under the dark condition at zero bias is calculated by using the following relation:

$$D^* = R\sqrt{\frac{R_0 A}{4k_B T}} \tag{2}$$

where R is the spectral responsivity, k_B is the Boltzmann constant, T is the temperature, A (cm^2) is the electrically active area of the detector, and R_0A is the resistance-area product at zero bias. The calculated value of D* for HE0204 and 15SP3 are shown in Fig. 4, and for more clarity of results, the full width at half maximum (FWHM) value of D* is also included in Fig. 4. It is observed that D* for peak as well as FWHM wavelength, range is higher in 15SP3 as compared to the

Table 2. Value of Peak and FWHM Responsivity and D* for HE0204 and 15SP3 at Temperature = 50 K.

Sample	Peak			FWHM		
	λ (μm)	R (A/W)	$D^*\times10^7$ (Jones)	λ range (μm)	R (A/W)	$D^*\times10^7$ (Jones)
15SP3	5.5	55.6×10^{-6}	15	4.0 - 8.9	28.3×10^{-6}	7.6
HE0204	11.6	20.3×10^{-3}	4.4	8.9 - 13.8	10.1×10^{-3}	2.2

HE0204. Moreover, the FWHM value of D* of 15SP3 is even higher than that of the peak value of D* at 11.6 μm of HE0204. All values are listed in Table II.

It may be noted here in this article that both HE0204 and 15SP3 have a difference of threshold wavelength ($16.1 - 13.7$ μm); however, there is an order of magnitude difference in the responsivity (i.e., HE0204 is of the order of mA/W, and 15SP3 is of the order of μA/W). Therefore, even for the same threshold wavelengths, a similar order of difference in order of responsivity is expected. Thus, the dark current advantage is stronger in ET detectors than the responsivity difference, giving rise to a better D*. Although the responsivity for the conventional device (HE0204) is higher, however, due to the reduced dark current, D* is higher for ET detector (15SP3). This confirms the proposed idea of longer threshold wavelength detector with a reduced dark current and D* advantage in ET detector as compared to a conventional detector.

IV. CONCLUSION

In conclusion, a conventional detector HE0204 have dark current and photoresponse threshold corresponding to designed $\Delta = 0.077$ eV, which gives $\lambda_t = 16.1$ μm at 50 K. However, as proposed ET detector 15SP3 has a dark current designed $\lambda_t = 3.1$ μm, whereas λ_{eff} corresponding to 13.7 μm at 50 K. This dark current advantage leads to the higher value of $D^* = 1.5 \times 10^8$ Jones for 15SP3 over HE0204 = 1.1×10^7 Jones, even though the responsivity of 15SP3 is much lower as compared to HE0204. On the basis of the results, it can be concluded that the ET detector can be designed to have a longer threshold wavelength with a reduced dark current and D* advantage. This idea can be further employed to reduce the energy consumption of most of the electronic components, leading to large scale savings, by reducing unwanted (as heat) energy usage.

ACKNOWLEDGMENT

This work was supported, in part, by the U.S. Army Research Office under Grant W911 NF-15-1-0018 and in part by the European Community's Seventh Framework Programme (FP7) under Grant 247375 "TOSCA."

REFERENCES

[1] Y. F. Lao, P. K. D. D. P. Pitigala, A. G. U. Perera, H. C. Liu, M. Buchanan, and Z. R. Wasilewski, "Light-hole and heavy-hole transitions for high-temperature long-wavelength infrared detection," *Appl. Phys. Lett.*, vol. 97, 2010, Art. no. 091104.

[2] D. G. Esaev, M. B. M. Rinzan, S. G. Matsik, and A. G. U. Perera, "Design and optimization of GaAs/AlGaAs heterojunction infrared detectors," *J. Appl. Phys.*, vol. 96, pp. 4588–4597, 2004.

[3] Y.-F. Lao, A. G. U. Perera, L. H. Li, S. P. Khanna, E. H. Linfield, and H. C. Liu, "Tunable hot-carrier photodetection beyond the bandgap spectral limit," *Nat. Photon.*, vol. 8, pp. 412–418, 2014.

[4] S. G. Matsik, M. B. M. Rinzan, D. G. Esaev, A. G. U. Perera, H. C. Liu, and M. Buchanan, "20 μm cut off heterojunction interfacial work function internal photoemission detectors," *Appl. Phys. Lett.*, vol. 84, pp. 3435–3437, 2004.

[5] D. Chauhan, A. G. U. Perera, L. H. Li, L. Chen, and E. H. Linfield, "Dark current and photoresponse characteristics of extended wavelength infrared photodetectors," *J. Appl. Phys.*, vol. 122, 2017, Art. no. 024501.

[6] Y.-F. Lao, P. Pitigala, A. U. Perera, L. Li, S. Khanna, and E. Linfield, "Wavelength-extended photovoltaic infrared photodetectors," *Appl. Phys. Lett.*, vol. 104, 2014, Art. no. 131101.

[7] D. Chauhan, A. G. U. Perera, L. Li, L. Chen, S. P. Khanna, and E. H. Linfield, "Extended wavelength infrared photodetectors," *Opt. Eng.*, vol. 56, pp. 091605–091605, 2017.

[8] D. Chauhan, A. G. U. Perera, L. Li, L. Chen, and E. H. Linfield, "Effects of barrier energy offset and gradient in extended wavelength infrared detectors," *IEEE Sens. Lett.*, vol. 2, no. 4, Dec. 2018, Art no. 3502104.

[9] D. Somvanshi, D. Chauhan, A. G. U. Perera, L. Li, L. Chen, and E. H. Linfield, "Analysis of barrier parameters on the extended threshold wavelength of infrared detectors," *IEEE Photon. Technol. Lett.*, vol. 30, no. 18, pp. 1617–1620, Sep. 2018.

[10] J. Shah, "Hot electrons and phonons under high intensity photoexcitation of semiconductors," *Solid-State Electron.*, vol. 21, pp. 43–50, 1978.

[11] J. Shah, "Hot carriers in quasi-2-D polar semiconductors," *IEEE J. Quantum Electron.*, vol. QE-22, no. 9, pp. 1728–1743, Sep. 1986.

[12] D. Somvanshi *et al.*, "Analysis of extended threshold wavelength photoresponse in nonsymmetrical p-GaAs/AlGaAs heterostructure photodetectors," *IEEE J. Sel. Topics Quantum Electron.*, vol. 24, no. 2, Mar./Apr. 2018, Art no. 3801407.

[13] B. Brill and M. Heiblum, "Electron heating in GaAs due to electron-electron interactions," *Phys. Rev. B*, vol. 49, pp. 14762–14765, 1994.

[14] K. Santra and C. K. Sarkar, "Energy-loss rate of hot carriers in semiconductors with nonequilibrium phonon distribution in the extreme quantum limit at low temperatures," *Phys. Rev. B*, vol. 47, pp. 3598–3602, 1993.

[15] K. J. Tielrooij, M. Massicotte, L. Piatkowski, A. Woessner, Q. Ma, and P. Jarillo-Herrero, "Hot-carrier photocurrent effects at graphene–metal interfaces," *J. Phys., Condens. Matter*, vol. 27, 2015, Art. no. 164207.

[16] J. R. M. Saavedra, A. Asenjo-Garcia, and F. J. García de Abajo, "Hot-electron dynamics and thermalization in small metallic nanoparticles," *ACS Photon.*, vol. 3, pp. 1637–1646, 2016.

[17] Y. F. Lao *et al.*, "Analysis of dark current mechanisms for split-off band infrared detectors at high temperatures," *IEEE Trans. Electron. Device*, vol. 57, no. 6, pp. 1230–1236, Jun. 2010.

[18] Y.-F. Lao and A. G. U. Perera, "Temperature-dependent internal photoemission probe for band parameters," *Phys. Rev. B*, vol. 86, 2012, Art. no. 195315.